Water Supply

Water Supply Vol 23 No 8, 3486 doi: 10.2166/ws.2023.193

Exploring efficient photocatalytic degradation of humic acid from aqueous solution with plant-based $ZnFe_2O_4$@TiO_2 magnetic nanocomposite using *Elaeagnus angustifolia* tree bark methanolic extract

Majid Asri[a], Ali Naghizadeh[b,*], Amirhesam Hasani[a], Sobhan Mortazavi-Derazkola[b], Amirhossein Javid[a] and Ali Yousefinia[b]

[a] Department of Environmental Engineering, Faculty of Natural Research and Environment, Science and Research Branch, Islamic Azad University, Tehran, Iran
[b] Medical Toxicology & Drug Abuse Research Center (MTDRC), Birjand University of Medical Sciences (BUMS), Birjand, Iran
*Corresponding author. E-mail: al.naghizadeh@yahoo.com

AN, 0000-0002-3015-2609

ABSTRACT

In the process of sanitizing drinking water, humic acid present in drinking water sources reacts with chlorine disinfectant and forms mutagenic, defective, and carcinogenic disinfection byproducts such as trihalomethanes and haloacetic acids. In the present study, the methanolic extract of *Elaeagnus angustifolia* tree bark was used for the synthesis of $ZnFe_2O_4$@TiO_2 nanocomposite and then properties and structural elements and diagnostic features of nanoparticles were analyzed. According to the results, the $ZnFe_2O_4$@TiO_2 nanocomposites have an average crystalline size of ~65–250 nm. Also, the effects of pH (3–11), nanoparticle dose (0.005–0.1 g/L), and humic acid concentration (2–15 mg/L) were examined up to 120 min of time. From the results, the highest removal percentages achieved about 100% at optimal conditions (pH = 3, nanocomposite dose = 0.05 g/L and humic acid initial concentration = 2 mg/L). The results of this research showed that the efficiency of nanocomposite at the highest concentration of humic acid that was investigated in this research (15 mg/L) was about 95.67%. Therefore, it can be concluded that this nanocomposite, while being cost-effective and environmentally friendly, is also very effective in removing humic acid from an aqueous solution.

Key words: *Elaeagnus angustifolia*, green synthesis, humic acid, photocatalytic degradation, $ZnFe_2O_4$@TiO_2

HIGHLIGHTS

- New magnetic $ZnFe_2O_4$@TiO_2 nanocomposite was synthesized and characterized.
- FT–IR, SEM, EDS, and XRD analyses showed the successful synthesis of $ZnFe_2O_4$@TiO_2 nanocomposite.
- In optimum condition, 100% degradation efficiency of humic acid was observed.

GRAPHICAL ABSTRACT

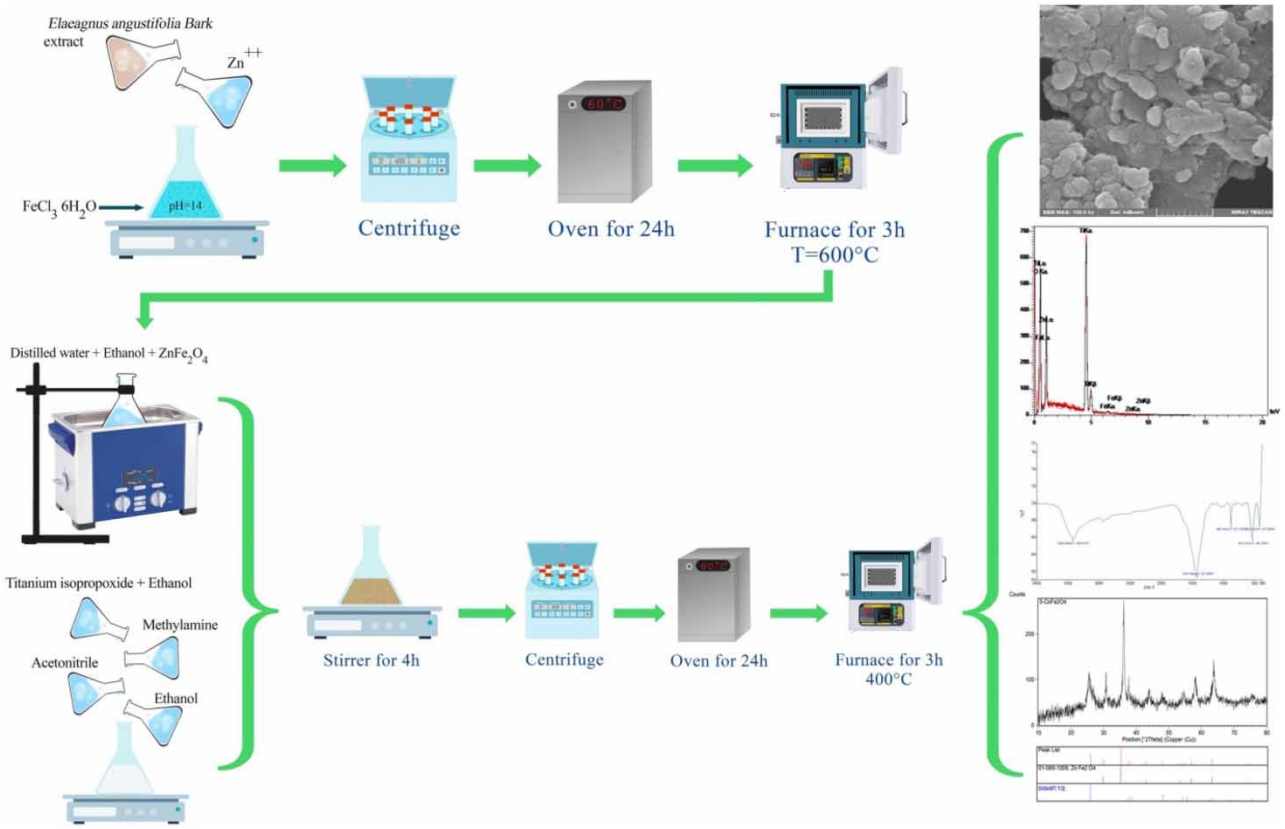

INTRODUCTION

Among the natural organic polyelectrolytes, humic and fulvic acids (HA and FA) can be mentioned, which constitute the largest proportion of naturally soluble organic substances in water systems (Thurman *et al.* 1982; Buffle 1990). They can generally be considered as belonging to three parts, HA, which precipitates at pH equal to or less than 2.0 but is soluble in alkaline to weakly acidic solutions (Naghizadeh *et al.* 2013a); Humin, which is insoluble in all pH values, and FA, which is soluble in water in all pH values (Katsumata *et al.* 2008). The color of humic substances is yellow to black and they have a high molecular weight (100 to several thousand daltons) (Palmer *et al.* 2002). Removing them from drinking water resources is of great importance because they can have a negative effect on the appearance and taste of water, and if they react with chlorine, they can cause the production of chlorinated organic compounds that have the potential to cause cancer. In addition, the presence of dissolved organic substances may reduce the performance of water purification processes in which microporous absorbents or membranes are used (Summers *et al.* 1989; Katsumata *et al.* 2008). Humic substances make up approximately 50% of natural organic substances in water (Katsumata *et al.* 2008).

There are different ways to remove HA in treatment plants, which can be done by filtration, ion-exchange, coagulation, precipitation, using activated carbon. activated carbon), or biological treatment as common methods of humic acid removal (Alborzfar *et al.* 1998; Ruohomäki *et al.* 1998; Naghizadeh *et al.* 2017). One of the problems of using the coagulation process to remove humic acid is the high consumption of coagulant materials and the production of high sludge, which increases the operating and maintenance costs in the water treatment process, and is one of the unfavorable features of the ion-exchange method for removing Natural organic compounds are slow reaction speed or process kinetics (Naghizadeh *et al.* 2015; Derakhshani *et al.* 2023). Also, studies indicate that the decomposition of humic acid can be occurred with different methods such as photochemical (Hustert *et al.* 1999), electrochemical (Motheo & Pinhedo 2000), photoelectrocatalytic (Selcuk *et al.* 2004), and heterogeneous photocatalysis (Wiszniowski *et al.* 2002).

Irradiation is one of the most efficient methods for removing pollutants from water and sewage, which is capable of removing non-biodegradable organic pollution and removing microbial pollution caused by viruses, bacteria, etc. Ionizing radiations such as UV rays, X-rays, gamma rays, and high-speed electrons are effective forms of energy that can remove organic pollutants from water and wastewater (Behjat *et al.* 2007). Photocatalytic oxidation is known as a successful purification process for the degradation of pollutants in water systems. One of the important features of this process is its effectiveness for the mineralization of the target compound, which is done by the mechanism of non-selective oxidation of hydroxyl radicals. So far, it has been proven that TiO_2 is the strongest photocatalyst (Linsebigler *et al.* 1995; Di Paola *et al.* 2012). TiO_2 is a nanostructured semiconductor whose very good photocatalytic activity is widely used (Bu *et al.* 2015; Wu *et al.* 2015; Zhang *et al.* 2015) and because of its non-toxicity, high stability, and low cost, it is one of the most promising catalytic materials under ultraviolet rays (Xu *et al.* 2015). Doping TiO_2 with metal ions leads to an increase in the rate of formation of OH radicals (Iwasaki *et al.* 2000). For this reason, in recent years, TiO_2 doping technique by metal ion has been widely studied (Ohno *et al.* 2004; Vargas *et al.* 2012; Hossein Panahi *et al.* 2020).

Among the investigated transition metal ions, Fe^{+3} can be a favorable case for doubling due to its radius similar to that of Ti^{4+}. In addition, the energy level of Fe^{2+}/Fe^{3+} is close to the energy level of Ti^{3+}/Ti^{4+} (Birben *et al.* 2017). In recent years, physicochemical properties and preparation methods of $ZnFe_2O_4/TiO_2$ composite have been taken into consideration in order to increase its photocatalytic activity. Methods, such as solution combustion method (Zhu *et al.* 2014), sol-gel method (Jiang *et al.* 2015), hydrothermal deposition method (Wang *et al.* 2013), and colloid chemical method (Quan *et al.* 2014).

Nowadays, due to the increase in environmental pollution and their harmful effects on the life of living organisms, the development of processes that reduce pollution in chemical synthesis is of great importance. Based on this, the development of chemical methods using catalysts, chemicals, solvents, and biocompatible processes is considered important in green chemistry (Maleki *et al.* 2018). One of the plant extracts that is important in traditional medicine in the world is Elaeagracea extract, which exists in the regions of North Asia to the Himalayas and Europe. Traditionally, its various species are used as therapeutic agents. For example, the ripe fruits of *Elaeagnus philippinensis* are used in the treatment of amoebic dysentery (Perry & Metzger 1980). In traditional Chinese medicine, the leaves of this plant are used to treat asthma, bronchitis, and other respiratory diseases (Goncharova *et al.* 1994). Also, in the traditional medicine of Korea, antibacterial, anti-diarrheal and anti-asthmatic properties are mentioned for it (Nishino *et al.* 1987).

In this study, the bark of the *Elaeagnus angustifolia* was used for the production of this nanocomposite for the first time. Properties and structural elements and diagnostic features of nanoparticles were analyzed by Fourier transform infrared spectroscopy (FT-IR), scanning electron microscope (SEM), X-ray diffraction (XRD), dynamic light scattering (DLS), and energy-dispersive X-ray spectrometry (EDS) analyses. Also, the photocatalytic activity of $ZnFe_2O_4@TiO_2$ nanocomposite made by the green method was tested with UV-C radiation to remove humic acid, and the optimal limit of factors affecting the process, including contact time, pH, humic acid concentration, and nanoparticle dose, was also investigated and reported.

MATERIALS AND METHODS

Green extraction and synthesis of magnetic nanocomposite

First, the barks of the *E. angustifolia* tree were collected. The leaves were dried and then extracted by percolation with methanol. In this way, in the beginning, the desired amount of the dried plant was immersed in the methanol solution and in the separating funnel. In such a way, that the methanol solution completely covered the dried plant. Then, every 12 h, the methanol solution was emptied and put back into the separating funnel. This operation continued for 3 days and nights. Then, after 3 days, the solution obtained from the plant extract and methanol was placed in the rotary device. By removing methanol from the solution, the intended extract was obtained from the plant.

Synthesis of $ZnFe_2O_4$ nanoparticles

First, 10 mL of distilled water was degased then 1 mMol of iron chloride compound $FeCl_3{\cdot}6\ H_2O$ was added at a temperature of 70–80 °C until it dissolves, and after a minute, 0.5 mMol of the extract obtained from the tree bark was added. The *E. angustifolia* was dissolved in 5 mL of ethylene glycol with 5 mL of distilled water and 0.5 mMol of metal salt (Zn) was added which was previously dissolved in 10 mL of distilled water and finally iron salt was added to the aqueous mixture. This reaction should proceed by raising the pH to 14 by adding NaOH 2 M for 3 h under stirrer conditions. Then, the sediments obtained by the magnet were separated from the solution and washed three times with water and three times with ethanol

and placed in an oven under a temperature of 80 °C for 24 h. Finally, the obtained powder was calcined at 600 °C for 3 h. The schematic of the green synthesis of $ZnFe_2O_4$ nanoparticles was shown in Figure 1.

Synthesis of $ZnFe_2O_4$@TiO_2 magnetic nanocomposites

First, in a container, 0.2 g of $ZnFe_2O_4$ synthesized in the previous step was dispersed in 30 mL of ethanol and distilled water under ultrasonic bath conditions for 30 min. In a separate container, 0.05 L of ethanol, 0.04 L of acetonitrile, 0.001 mol of methylamine, and 0.024 mol of distilled water were mixed together completely. Then 0.006 mol of titanium tetraisopropoxide was dissolved in 0.01 L of ethanol solution and added to the prepared mixture. The resulting product was a white suspension. After 60 min of vigorous stirring, the product obtained in this step was added to the reaction vessel containing Zn. After 4 h, the sample was washed and dried. Finally, it was calcined at 400 °C for 3 h (Mohammadi *et al.* 2022). The schematic of the green synthesis of $ZnFe_2O_4$@ TiO_2 nanocomposite was shown in Figure 2.

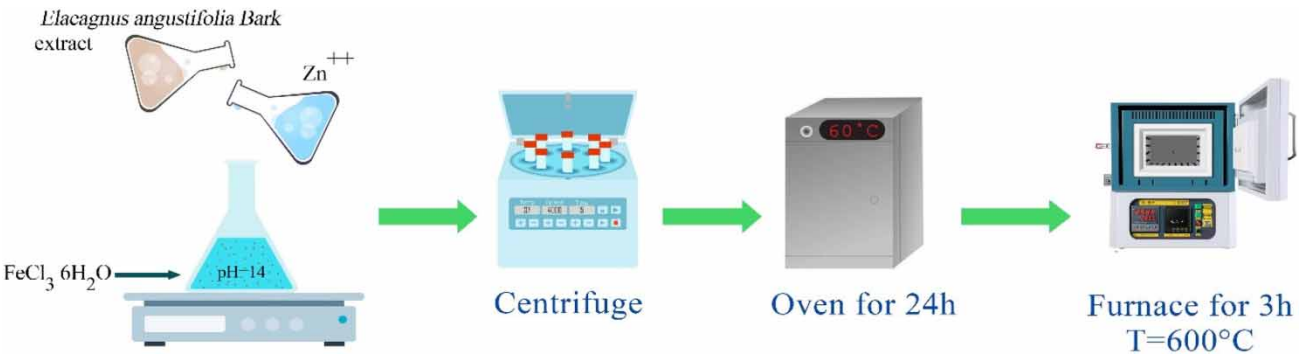

Figure 1 | Green synthesis of $ZnFe_2O_4$ nanoparticles.

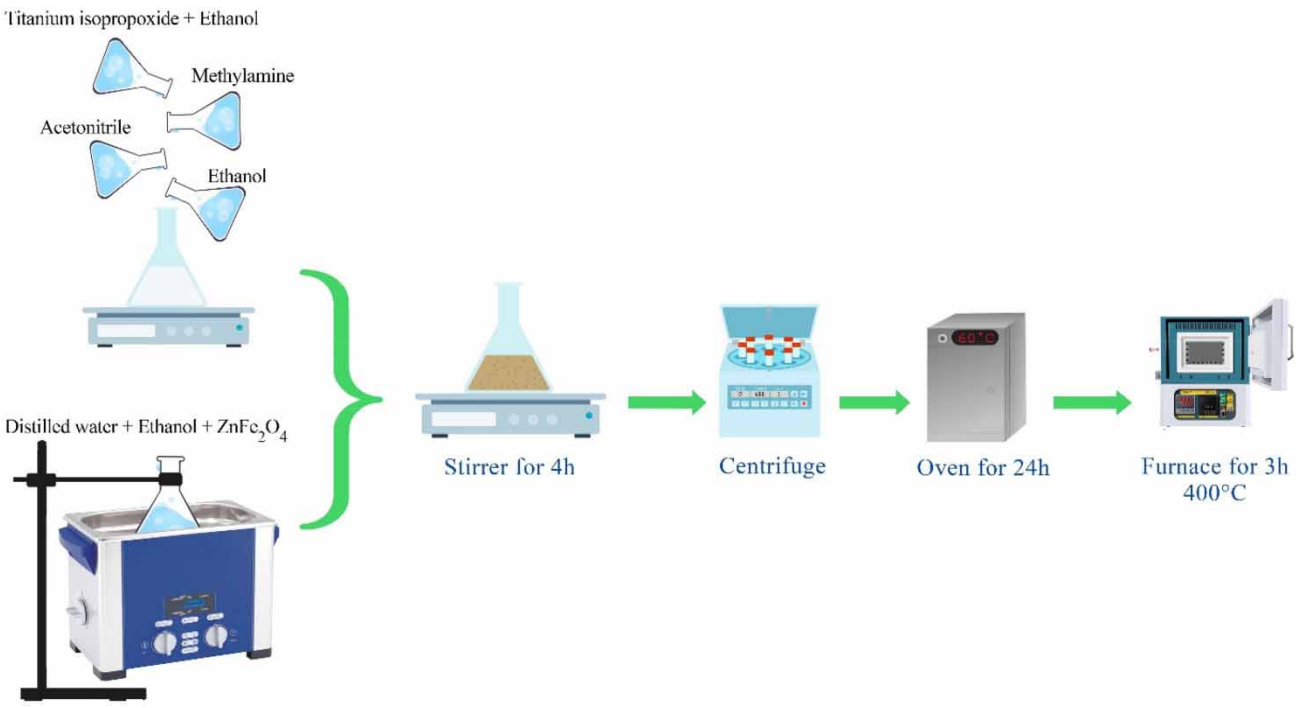

Figure 2 | Synthesis of $ZnFe_2O_4$@TiO_2 magnetic nanocomposites.

Humic acid photocatalytic degradation experiments:

The photocatalytic degradation test of $ZnFe_2O_4@TiO_2$ magnetic nanocomposites was performed in the presence of ultraviolet light. Different concentrations of humic acid were poured in a certain volume inside the pilot and a specific mass of synthesized $ZnFe_2O_4@TiO_2$ nanocomposite was added to this solution. Before turning on the lamp and irradiating UV-C light, the desired solution is aerated for 30 min in the dark with stirring in order to balance absorption and desorption with oxygen. Then the UV lamp was turned on and the amount of humic acid removal was measured by changing different variables. During the photocatalytic process, aeration was performed to mix the contents of the pilot. After a certain period of time, a sample was taken from the solution inside the pilot and the amount of humic acid degradation was measured by UV–Vis spectrophotometry device at a wavelength of 254 nm. Then, using the following relationship, the percentage of humic acid degradation was determined:

$$D(\%) = \frac{C_0 - C_t}{C_0} \times 100$$

where D (%) represents the percentage of humic acid degradation by photocatalytic process; C_0 is the initial concentration of humic acid in mg/L; C_t is the final concentration of humic acid sampled from the pilot after UV light irradiation.

Determining the effect of pH

In this step, in order to determine the optimal pH, the pH of the acidic solution was adjusted to 3, 5, 7, 9, and 11 using a pH meter using HCl and NaOH (0.1 N). Then, by keeping other parameters affecting the analysis constant (nanoparticle dose, contact time and humic acid concentration), a certain amount of $ZnFe_2O_4@TiO_2$ nanocomposite was weighed and added to the solution and exposed to UV rays in the reactor. After the specified contact time, sampling was done from the pilot valve and after separating the nanocomposite from the solution, the humic acid concentration was measured by a spectrophotometer. The highest amount of humic acid decomposition (the lowest residual concentration of humic acid in the solution leaving the pilot) at any pH that occurs was selected as the optimum pH.

Determining the effect of contact time

After determining the optimum pH, the amount of decomposition was determined for each contact time of 5, 10, 20, 40, 60, and 90 min while keeping other parameters constant by adding 0.05 mg of $ZnFe_2O_4@TiO_2$.

Determining the effect of nanoparticle dose

After determining the optimal pH and contact time from the previous steps, acidomic decomposition by adding specific doses of $ZnFe_2O_4@TiO_2$ nanocomposite (0.005, 0.01, 0.02, 0.03, 0.04, 0.05, and 0.1 g/L) was measured in the humic acid solution inside the pilot. Any dose of nanocomposite that had the highest degradation of humic acid was selected as the optimal dose.

Determining the characteristics of $ZnFe_2O_4@TiO_2$ nanocomposite

In order to determine the characteristics of the synthesized nanocomposite and ensure its effective synthesis, various techniques such as FESEM (Tescan Mira3 FESEM, Czech Republic), XRD (Philips, PW1730, Holland) device with Cu Kαradiation ($K = 1.5406$ A°), DLS (NanoBrook 90Plus Pals), EDS and FT–IR (JASCO, FT/IR-4600, Japan) were performed.

RESULTS AND DISCUSSION

Structural analysis

Scanning electron microscope

An SEM was used to determine the surface structure of the sample. The SEM image of $ZnFe_2O_4@TiO_2$ in Figure 3 shows that the synthesized products of nanocrystals of spherical shape particles and oval morphology are well crystallized, which have accumulated together due to the presence of magnetic interactions between the particles. When TiO_2 nanoparticles were placed on $ZnFe_2O_4$ surface, the size of nanoparticles increased. As shown in the picture, the nanoparticles have a spherical morphology and are strongly accumulated. On the other hand, in the study of Mirzaei *et al.*, the $ZnFe_2O_4@TiO_2$/Cu particles were somewhat aggregated, and one of the reasons for that was the strong magnetic property between the $ZnFe_2O_4$ particles and their magnetic dipole interaction (Mirzaee *et al.* 2008).

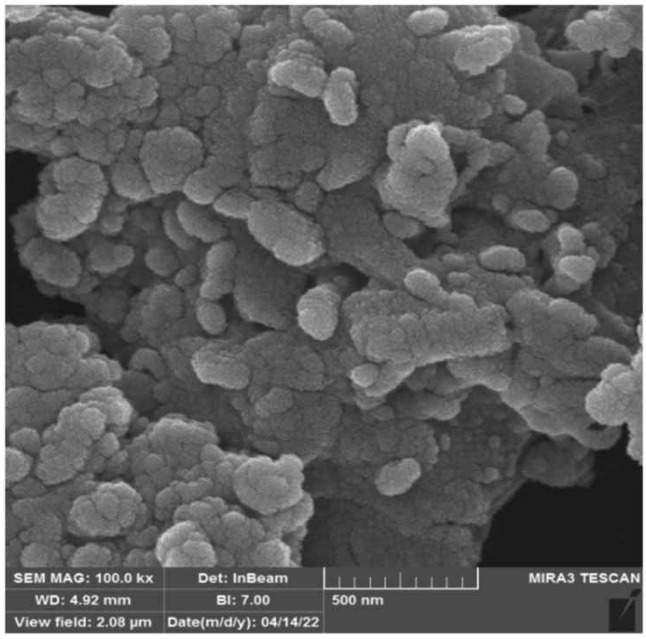

Figure 3 | The SEM image of $ZnFe_2O_4$@TiO_2 nanocomposite.

X-ray diffraction

The crystal structure of the synthesized materials was determined by XRD analysis. The XRD pattern of the $ZnFe_2O_4$@TiO_2 nanoparticle in Figure 4 shows that in addition to the diffraction peaks caused by the $ZnFe_2O_4$ component, additional diffraction peaks are observed at 26.2°, 38.1°, 48.5°, 54.3°, 55.7° (2θ) pages (1) 0 1), (0 0 4), (2 0 0), (1 0 5), and (2 1 1) of TiO_2 with anatase structure (JCPDS: 004-004-0477). All the diffraction peaks of $ZnFe_2O_4$ nanoparticles match the pattern of JCPDS database number: 1150-79 (Zhang *et al.* 2012). The XRD peaks of TiO_2 nanobelts correspond to the anatase phase and correspond well with the JCPDS standard pattern number: 1272-21 (Zhou *et al.* 2010).

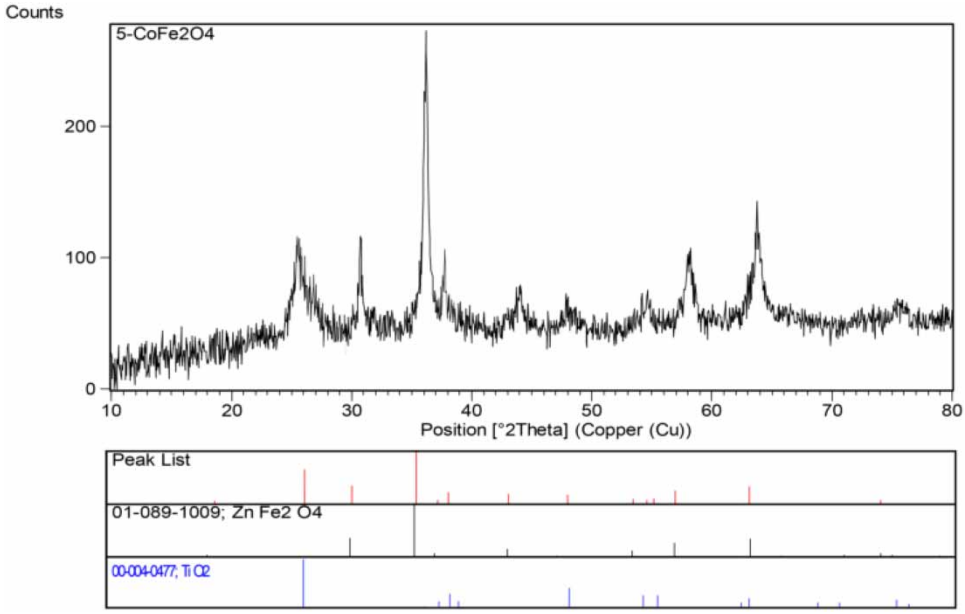

Figure 4 | The XRD pattern of $ZnFe_2O4$@TiO_2 nanocomposite.

Dynamic light scattering

Surface charge and size distribution of $ZnFe_2O_4@TiO_2$ nanocomposite were calculated through zeta potential and DLS analysis, respectively. The histogram of DLS analysis for the particle size distribution of the prepared $ZnFe_2O_4@TiO_2$ is shown in Figure 5. DLS analysis showed that the average size of $ZnFe_2O_4@TiO_2$ was approximately 65–250 nm. Also, the zeta potential of the synthesized magnetic $ZnFe_2O_4@TiO_2$ was −30.7 mV (Figure 5). Uniformity of size distribution is an excellent characteristic of composites because it can be directly related to the properties and reactivity of nanocomposite (Ahmadpour *et al.* 2020).

Energy-dispersive X-ray spectrometry

EDS is a method to determine the percentage of elements in a sample (Ahmadpour *et al.* 2020). As seen in Figure 6, EDS analysis was performed to determine the elemental composition of $ZnFe_2O_4@TiO_2$ and check the obtained spectrum for the presence of zinc (Zn), iron (Fe), titanium (Ti) elements, and confirmed oxygen (O). In addition, EDS elemental mapping of $ZnFe_2O_4@TiO_2$ nanoparticles shows that the elements are evenly distributed.

FT–IR

Infrared spectroscopy (FT–IR) of $ZnFe_2O_4@TiO_2$ nanocomposite is presented in Figure 7. The broad peaks at about 3,400 cm and the compact peak at about 1,600 cm are related to the stretching and bending vibration of water molecules, respectively. In addition, an obvious peak around 760 cm^{-1} is attributed to the vibration of the Zn–O bond (Figure 7). Also, in his study, Zang found the bond vibrations in the range of 550–415 cm^{-1} to be related to Zn–O and Fe–O stretching vibrations, which

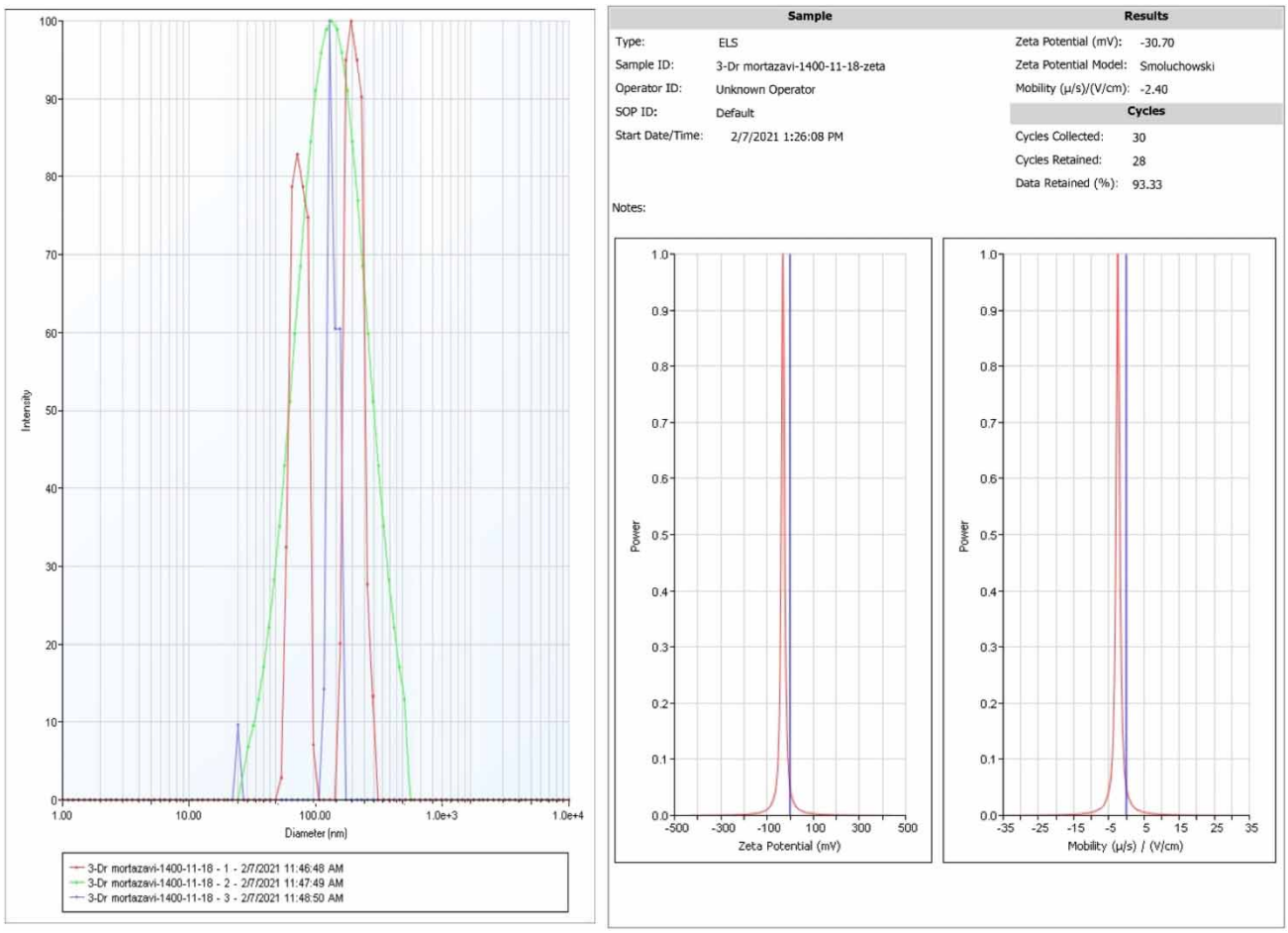

Figure 5 | The DLS analysis of $ZnFe_2O_4@TiO_2$ nanocomposite.

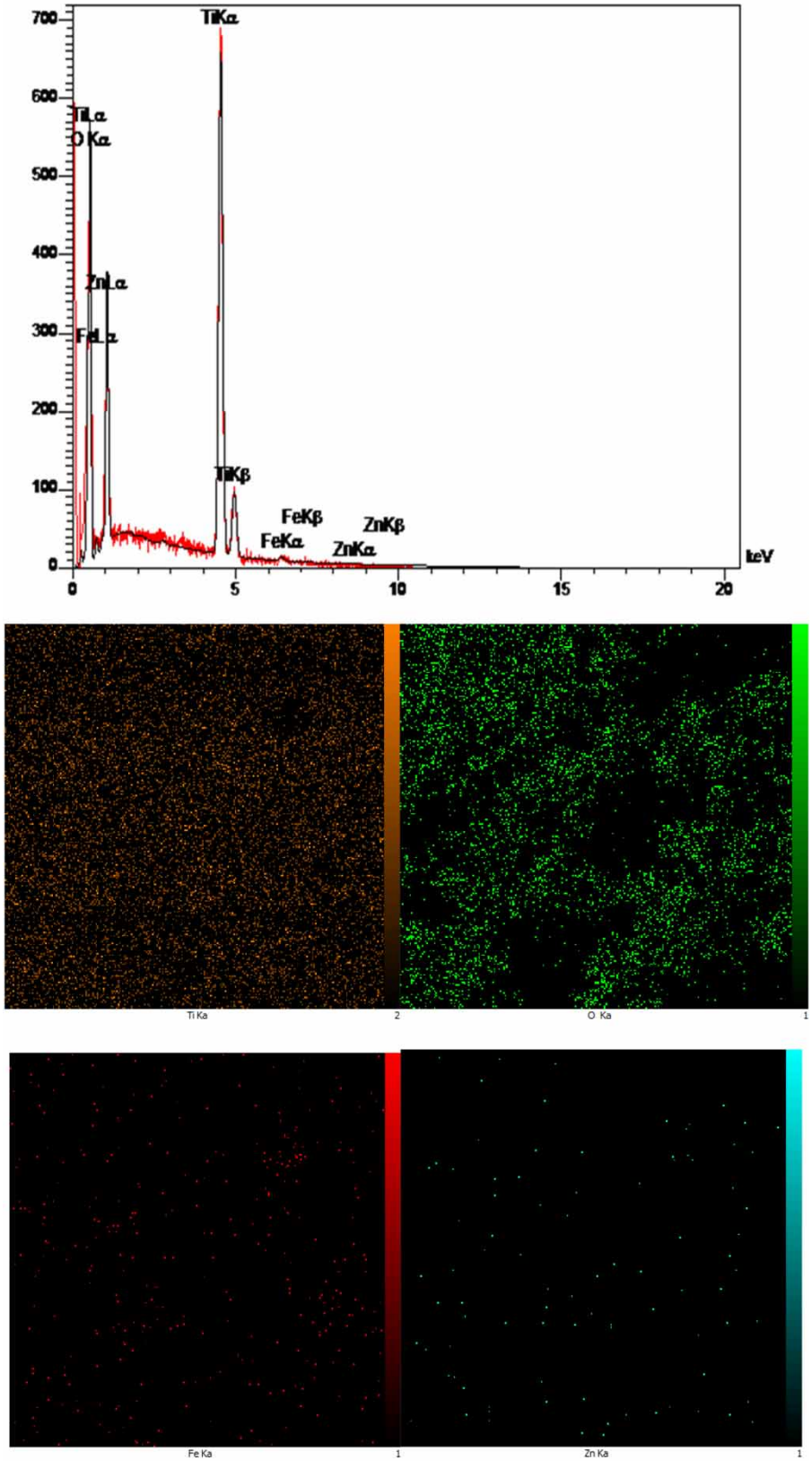

Figure 6 | The EDS and mapping analysis of $ZnFe_2O4@TiO_2$ nanocomposite.

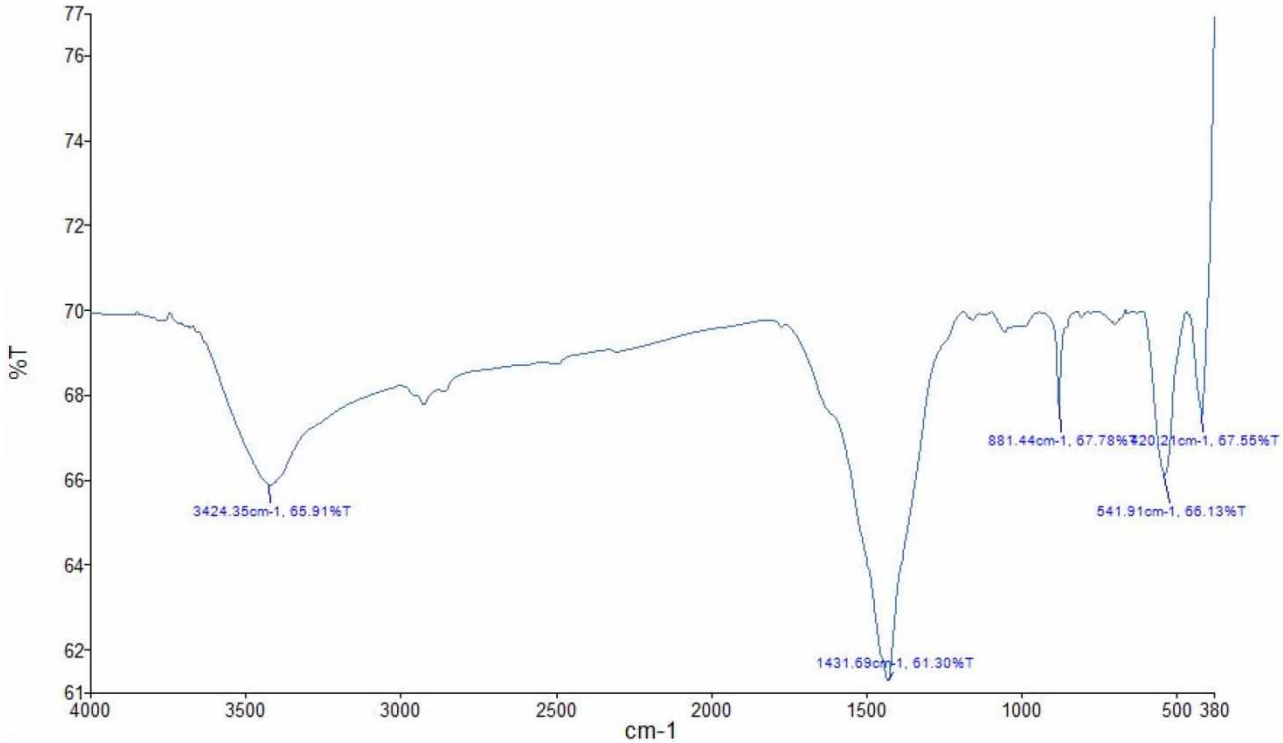

Figure 7 | The FT–IR spectrum of $ZnFe_2O_4@TiO_2$ nanocomposite.

shows the structure of zinc ferrite (Zhang *et al.* 2014). Also, the 3,400 cm^{-1} peak is related to O–H stretching vibrations (Khashan *et al.* 2017).

FT–IR spectrum of $ZnFe_2O_4@TiO_2$ nanocomposites is shown in Figure 7. In this spectrum, the bonding of magnetic materials is observed at the peak of 900–400 cm^{-1} (Ti–O, Zn–O, and Fe–O bonds). The band at 1451 is assigned to C–H bending modes. Also, the general schematic green synthesis and structural properties of $ZnFe_2O_4@TiO_2$ nanocomposite was shown in Figure 8.

Effect of variable parameters on HA degradation

pH_{PZC}

The point of zero charge (PZC) is the pH of the suspension at which the net charge on the surface of an insoluble oxide/hydroxide is zero. PZC plays an important role in surface characterization of metal oxides/hydroxides. When the pH of the solution is higher than pH_{pzc} (PZC), the negative charge on the surface provides electrostatic interactions that are favorable for adsorbing cationic species (Naghizadeh *et al.* 2013b). As shown in Figure 9, the pH_{ZPC} of $ZnFe_2O_4@TiO_2$ nanocomposite was about 7. Therefore the surface of nanocomposite is negatively charged when exposed to $pH \geq 7$.

Effect of reaction time and pH

The initial pH is one of the most effective parameters in the photocatalytic process, so that by affecting the surface charge characteristics of the photocatalyst, it determines the state of ionization of the catalyst surface and affects the adsorption/desorption capacity of the target organic compounds (Safari *et al.* 2015). The removal of humic acids is pH-dependent because they contain both hydrophilic and hydrophobic functional groups (eg, carboxyl, carbonyl, phenolic, and alcohol forms) (Ashrafi *et al.* 2021). As shown in the figure, the removal efficiency of nanocomposite is higher at acidic pH and the highest is related to $pH = 3$.

The increased removal of humic acid at acidic pH (3) is in response to the presence of acidic ions of $H+$ (hydrogen) that increased the formation of •H radicals, it can be generated in three ways: (1) when cavities react with water molecules in pairs of electron–holes to form •OH and •H; (2) when •OH attacks the aromatic ring and breaks apart the bonded carbon-hydrogen

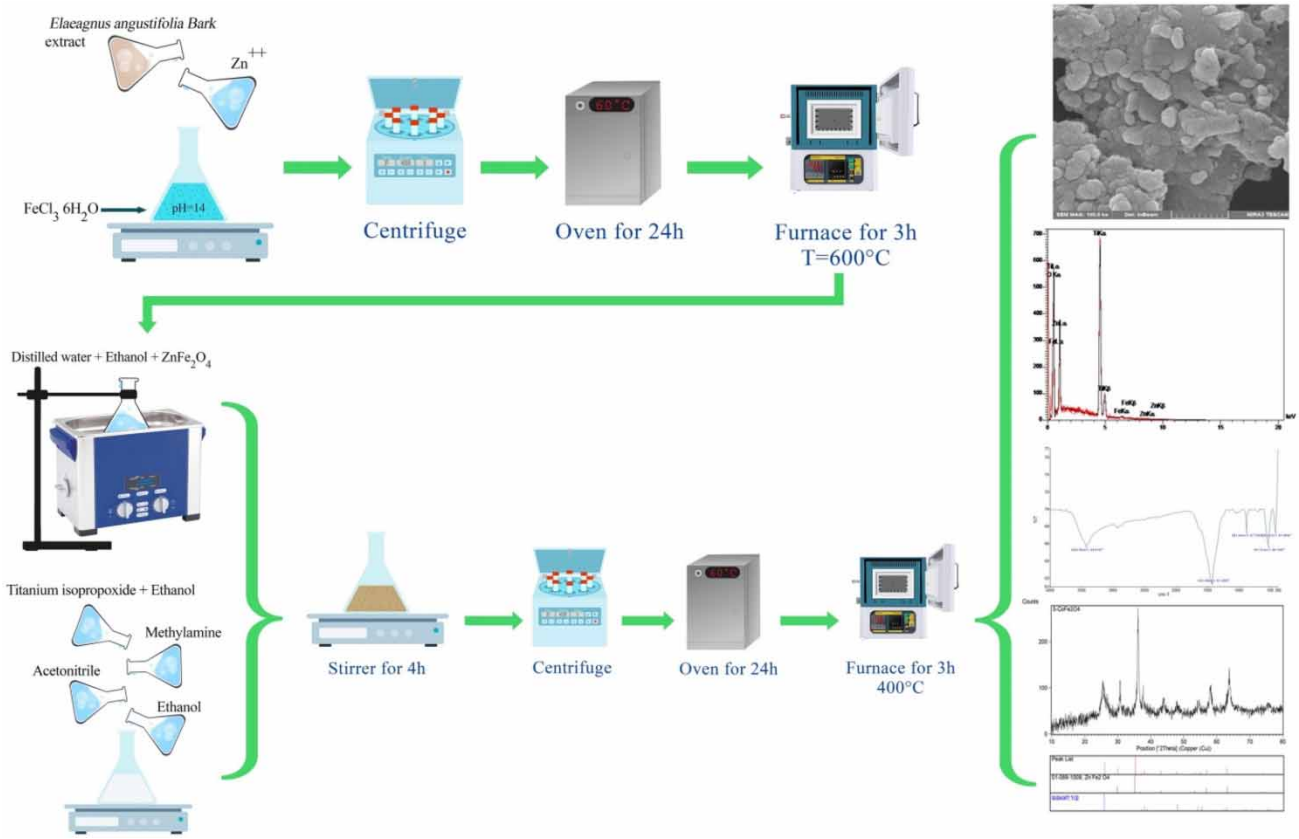

Figure 8 | The schematic green synthesis and structural properties of $ZnFe_2O_4@TiO_2$ nanocomposite.

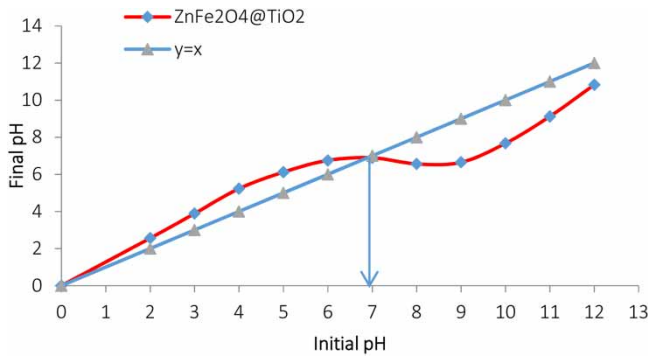

Figure 9 | The pH_{zpc} of $ZnFe_2O_4@TiO_2$ nanocomposite.

so that hydrogen forms •OH and •H; UV light is required to supply the energy to break the covalent bonds; (3) when H and •H form HO2 radicals using the oxygen present in solution to eventually form •OH radicals (Oskoei *et al.* 2016).

Effect of dose of $ZnFe_2O_4@TiO_2$ nanocomposite

In order to find the optimal concentration of nanocomposite and its highest decontamination efficiency, different concentrations of nanocomposite to remove the fixed amount of humic acid soluble in water and the optimal pH selected in the previous step (pH = 3) were tested and investigated, in the meantime, according to Figure 10, Nanocomposite with a concentration of 0.05 g/L showed the highest removal efficiency. Regarding the reaction time, according to the Figure 11, it can be

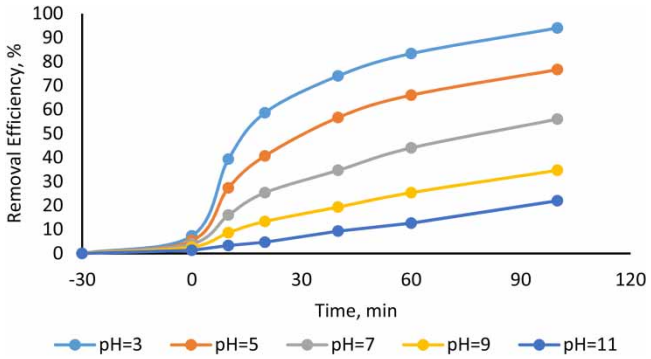

Figure 10 | Effect of dose of $ZnFe_2O_4@TiO_2$ nanocomposite in photocatalytic degradation of HA by $ZnFe_2O_4@TiO_2$ nanocomposite.

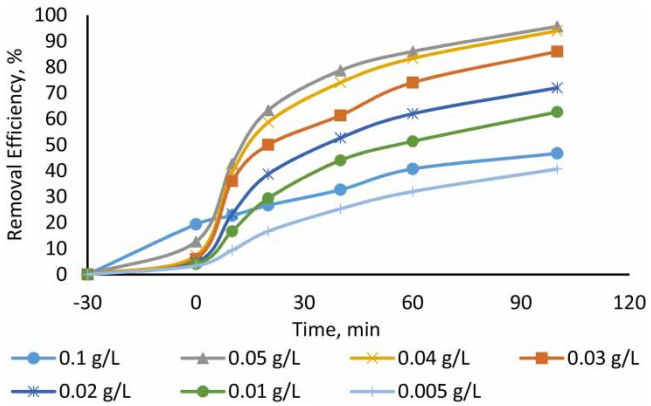

Figure 11 | Effect of reaction time and pH in photocatalytic degradation of HA by $ZnFe_2O_4@TiO_2$ nanocomposite.

concluded that humic acid degrades at a faster rate during the initial reaction time, especially the first 20 min, and the rate of degradation is close to constant from the 30th minute onwards.

As can be seen, according to the concentration of the catalyst, the removal efficiency increases up to a certain level, and after that, the removal efficiency occurs at a slower rate which indicates saturated photon absorption (Kamani *et al.* 2017; Mugunthan *et al.* 2018).

Effect of humic acid concentration

After conducting experiments and finding the optimal pH value and nanoparticle dose, different concentrations of humic acid to find the highest degradation rate in the time intervals specified in Figure 12, was tested and investigated. The

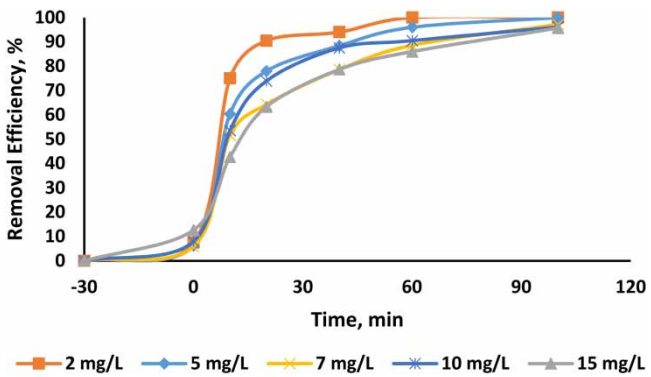

Figure 12 | Effect of humic acid concentration in photocatalytic degradation of HA by $ZnFe_2O_4@TiO_2$ nanocomposite.

nanocomposite dose and the tested pH are the same as the optimal value determined in the previous steps. As it is clear in Figure 12 generally, the removal process improves with the decrease of the concentration. Concentrations of 7 and 10 mg/L behaved like the above sentence. In general, the concentration of 2 mg/L was chosen as the optimal concentration of the pollutant. In their study, Kim *et al.* (2016) report that increasing the amount of humic acid molecules may also stop some of the light from reaching the photocatalyst surface, which can be seen from the results of this experiment. $ZnFe_2O_4$, a narrow band gap semiconductor (1.9 eV) has been used as a catalyst in the photocatalytic degradation of pollutants. Considering the relatively small band gap, $ZnFe_2O_4$ can be a good candidate for the photocatalytic degradation of organic pollutants in water (Valenzuela *et al.* 2002; Nikolić *et al.* 2012).

CONCLUSION

Magnetic $ZnFe_2O_4$@TiO_2 was synthesized by the green method using *E. angustifolia* tree bark methanolic extract. The green synthesized $ZnFe_2O_4$@TiO_2 nanocomposite was synthesis and characterized with different analyses. Also, the effects of different parameters on the photocatalytic degradation process were investigated under UV-C Light. The results of humic acid degradation by the $ZnFe_2O_4$@TiO_2 nanocomposite showed that this nanocomposite has a very good catalytic activity in the presence of UV light even at high HA concentrations. Therefore this nanocomposite can be used as a suitable catalyst in the removal and degradation of humic acid from aqueous solution.

ETHICAL APPROVAL

This paper was approved by the related ethical committee.

AUTHORS' CONTRIBUTIONS

M. A. wrote the draft of the paper. A. N. was the supervisor of this research project and contributed to conception and design of the work. A. H. and S. M. contributed to acquisition and analysis of the data. A. J. and A. Y. contributed to substantively revise the work. All authors read and approved the final manuscript.

FUNDING

The authors declare that no funds, grants, or other support were received during the preparation of this manuscript.

DATA AVAILABILITY STATEMENT

All relevant data are included in the paper or its Supplementary Information.

CONFLICT OF INTEREST

The authors declare there is no conflict.

REFERENCES

Ahmadpour, N., Sayadi, M. H., Sobhani, S. & Hajiani, M. 2020 A potential natural solar light active photocatalyst using magnetic $ZnFe_2O_4$ @ TiO_2/Cu nanocomposite as a high performance and recyclable platform for degradation of naproxen from aqueous solution. *Journal of Cleaner Production* **268**, 122023.

Alborzfar, M., Jonsson, G. & Grøn, C. 1998 Removal of natural organic matter from two types of humic ground waters by nanofiltration. *Water Research* **32**, 2983–2994.

Ashrafi, S. D., Safari, G. H., Sharafi, S., Kamani, H. & Jaafari, J. 2021 Adsorption of 4-Nitrophenol on calcium alginate-multiwall carbon nanotube beads: modeling, kinetics, equilibriums and reusability studies. *International Journal of Biological Macromolecules* **185**, 66–76.

Behjat, A., Mozahheb, S. A., Khalili, M. B., Vakhshoor, B., Zareshaei, H. & Fallahzadeh, M. 2007 Advanced oxidation treatment of drinking water and wastewater using high-energy electron beam irradiation. *Journal of Water and Wastewater; Ab va Fazilab (in Persian)* **18**, 60–68.

Birben, N. C., Uyguner-Demirel, C. S., Kavurmaci, S. S., Gürkan, Y. Y., Turkten, N., Cinar, Z. & Bekbolet, M. 2017 Application of Fe-doped TiO_2 specimens for the solar photocatalytic degradation of humic acid. *Catalysis Today* **281**, 78–84.

Bu, X., Wang, Y., Li, J. & Zhang, C. 2015 Improving the visible light photocatalytic activity of TiO_2 by combining sulfur doping and rectorite carrier. *Journal of Alloys and Compounds* **628**, 20–26.

BUFFLE, J. 1990 The analytical challenge posed by fulvic and humic compounds. *Analytica Chimica Acta* **232**, 1–2.

Derakhshani, E., Naghizadeh, A. & Mortazavi-Derazkola, S. 2023 Biosynthesis of $MnFe_2O_4$@ TiO_2 magnetic nanocomposite using oleaster tree bark for efficient photocatalytic degradation of humic acid in aqueous solutions. *Environmental Science and Pollution Research* **30**, 3862–3871.

Di Paola, A., García-López, E., Marcì, G. & Palmisano, L. 2012 A survey of photocatalytic materials for environmental remediation. *Journal of Hazardous Materials* **211**, 3–29.

Goncharova, N., Plugar', V., Rashkes, Y. V., Isamukhamedov, A. S. & Glushenkova, A. 1994 Oxygenated fatty acids of the seeds of *Elaeagnus angustifolia*. *Chemistry of Natural Compounds* **30**, 661–665.

Hossein Panahi, A., Meshkinian, A., Ashrafi, S. D., Naghizadeh, A., Abi, G. & Kamani, H. 2020 Survey of sono-activated persulfate process for treatment of real dairy wastewater. *International Journal of Environmental Science and Technology* **17**, 93–98.

Hustert, K., Moza, P. & Kettrup, A. 1999 Photochemical degradation of carboxin and oxycarboxin in the presence of humic substances and soil. *Chemosphere* **38**, 3423–3429.

Iwasaki, M., Hara, M., Kawada, H., Tada, H. & Ito, S. 2000 Cobalt ion-doped TiO_2 photocatalyst response to visible light. *Journal of Colloid and Interface Science* **224**, 202–204.

Jiang, Z., Jiang, D., Z, Y. A. N., Liu, D., Qian, K. & Xie, J. 2015 A new visible light active multifunctional ternary composite based on TiO_2–In_2O_3 nanocrystals heterojunction decorated porous graphitic carbon nitride for photocatalytic treatment of hazardous pollutant and H_2 evolution. *Applied Catalysis B: Environmental* **170**, 195–205.

Kamani, H., Bazrafshan, E., Ashrafi, S. D. & Sancholi, F. 2017 Efficiency of sono-nano-catalytic process of TiO_2 nano-particle in removal of erythromycin and metronidazole from aqueous solution. *Journal of Mazandaran University of Medical Sciences* **27**, 140–154.

Katsumata, H., Sada, M., Kaneco, S., Suzuki, T., Ohta, K. & Yobiko, Y. 2008 Humic acid degradation in aqueous solution by the photo-Fenton process. *Chemical Engineering Journal* **137**, 225–230.

Khashan, S., Dagher, S., Tit, N., Alazzam, A. & Obaidat, I. 2017 Novel method for synthesis of Fe_3O_4@TiO_2 core/shell nanoparticles. *Surface and Coatings Technology* **322**, 92–98.

Kim, J. K., Jang, D. G., Campos, L. C., Jung, Y. W., Kim, J.-H. & Joo, J. C. 2016 Synergistic removal of humic acid in water by coupling adsorption and photocatalytic degradation using TiO_2/coconut shell powder composite. *Journal of Nanomaterials* Hindawi Publishing Corporation 7109015, 1–10

Linsebigler, A. L., Lu, G. & Yates JR, J. T. 1995 Photocatalysis on TiO_2 surfaces: principles, mechanisms, and selected results. *Chemical Reviews* **95**, 735–758.

Maleki, A., Firouzi-Haji, R. & Hajizadeh, Z. 2018 Magnetic guanidinylated chitosan nanobiocomposite: a green catalyst for the synthesis of 1, 4-dihydropyridines. *International Journal of Biological Macromolecules* **116**, 320–326.

Mirzaee, O., Golozar, M. & Shafyei, A. 2008 Influence of V_2O5 as an effective dopant on the microstructure development and magnetic properties of Ni0.64Zn0.36Fe_2O_4 soft ferrites. *Materials Characterization* **59**, 638–641.

Mohammadi, N., Allahresani, A. & Naghizadeh, A. 2022 Enhanced photo-catalytic degradation of natural organic matters (NOMs) with a novel fibrous silica-copper sulfide nanocomposite (KCC1-CuS). *Journal of Molecular Structure* **1249**, 131624.

Motheo, A. J. & Pinhedo, L. 2000 Electrochemical degradation of humic acid. *Science of the Total Environment* **256**, 67–76.

Mugunthan, E., Saidutta, M. B. & Jagadeeshbabu, P. E. 2018 Visible light assisted photocatalytic degradation of diclofenac using TiO_2-WO_3 mixed oxide catalysts. *Environmental Nanotechnology, Monitoring & Management* **10**, 322–330.

Naghizadeh, A., Nasseri, S., Mahvi, A. H., Kalantary, R. R. & Rashidi, A. 2013a Continuous adsorption of natural organic matters in a column packed with carbon nanotubes. *Journal of Environmental Health Science and Engineering* **11**, 14.

Naghizadeh, A., Nasseri, S., Rashidi, A., Rezaei Kalantary, R., Nabizadeh, R. & Mahvi, A. 2013b Adsorption kinetics and thermodynamics of hydrophobic natural organic matter (NOM) removal from aqueous solution by multi-wall carbon nanotubes. *Water Science and Technology: Water Supply* **13**, 273–285.

Naghizadeh, A., Nasseri, S., Mahvi, A. H., Nabizadeh, R. & Kalantary, R. R. 2015 Fenton regeneration of humic acid-spent carbon nanotubes. *Desalination and Water Treatment* **54**, 2490–2495.

Naghizadeh, A., Momeni, F. & Derakhshani, E. 2017 Efficiency of ultrasonic process in regeneration of graphene nanoparticles saturated with humic acid. *Desalination and Water Treatment* **70**, 290–293.

Nikolić, M. V., Slankamenac, M., Nikolić, N., Sekulić, D., Aleksić, O. S., Mitrić, M., Ivetić, T. & Pavlović, V. B. 2012 Study of dielectric behavior and electrical properties of hematite α-Fe_2O_3 doped with Zn. *Science of Sintering* **44**, 307–321.

Nishino, C., Enoki, N., Tawata, S., Mori, A., Kobayashi, K. & Fukushima, M. 1987 Antibacterial activity of flavonoids against *Staphylococcus* epidermidis, a skin bacterium. *Agricultural and Biological Chemistry* **51**, 139–143.

Ohno, T., Akiyoshi, M., Umebayashi, T., Asai, K., Mitsui, T. & Matsumura, M. 2004 Preparation of S-doped TiO_2 photocatalysts and their photocatalytic activities under visible light. *Applied Catalysis A: General* **265**, 115–121.

Oskoei, V., Dehghani, M. H., Nazmara, S., Heibati, B., Asif, M., Tyagi, I., Agarwal, S. & Gupta, V. K. 2016 Removal of humic acid from aqueous solution using UV/ZnO nano-photocatalysis and adsorption. *Journal of Molecular Liquids* **213**, 374–380.

Palmer, F. L., Eggins, B. R. & Coleman, H. M. 2002 The effect of operational parameters on the photocatalytic degradation of humic acid. *Journal of Photochemistry and Photobiology A: Chemistry* **148**, 137–143.

Perry, L. M. & Metzger, J. 1980 Medicinal Plants of East and Southeast Asia: Attributed Properties and Uses. MIT press.

Quan, F., Hu, Y., Zhang, X. & Wei, C. 2014 Simple preparation of Mn-N-codoped TiO_2 photocatalyst and the enhanced photocatalytic activity under visible light irradiation. *Applied Surface Science* **320**, 120–127.

Ruohomäki, K., Väisänen, P., Metsämuuronen, S., Kulovaara, M. & Nyström, M. 1998 Characterization and removal of humic substances in ultra-and nanofiltration. *Desalination* **118**, 273–283.

Safari, G. H., Hoseini, M., Seyedsalehi, M., Kamani, H., Jaafari, J. & Mahvi, A. H. 2015 Photocatalytic degradation of tetracycline using nanosized titanium dioxide in aqueous solution. *International Journal of Environmental Science and Technology* **12**, 603–616.

Selcuk, H., Sene, J., Sarikaya, H., Bekbolet, M. & Anderson, M. 2004 An innovative photocatalytic technology in the treatment of river water containing humic substances. *Water Science and Technology* **49**, 153–158.

Summers, R. S., Haist, B., Koehler, J., Ritz, J., Zimmer, G. & Sontheimer, H. 1989 The influence of background organic matter on GAC adsorption. *Journal-American Water Works Association* **81**, 66–74.

Thurman, E., Wershaw, R., Malcolm, R. & Pinckney, D. 1982 Molecular size of aquatic humic substances. *Organic Geochemistry* **4**, 27–35.

Valenzuela, M., Bosch, P., Jiménez-Becerrill, J., Quiroz, O. & Páez, A. 2002 Preparation, characterization and photocatalytic activity of ZnO, Fe_2O_3 and $ZnFe_2O_4$. *Journal of Photochemistry and Photobiology A: Chemistry* **148**, 177–182.

Vargas, X., Tauchert, E., Marin, J.-M., Restrepo, G., Dillert, R. & Bahnemann, D. 2012 Fe-doped titanium dioxide synthesized: photocatalytic activity and mineralization study for azo dye. *Journal of Photochemistry and Photobiology A: Chemistry* **243**, 17–22.

Wang, M., Sun, L., Cai, J., Huang, P., Su, Y. & Lin, C. 2013 A facile hydrothermal deposition of $ZnFe_2O_4$ nanoparticles on TiO_2 nanotube arrays for enhanced visible light photocatalytic activity. *Journal of Materials Chemistry A* **1**, 12082–12087.

Wiszniowski, J., Robert, D., Surmacz-Gorska, J., Miksch, K. & Weber, J.-V. 2002 Photocatalytic decomposition of humic acids on TiO_2: part I: discussion of adsorption and mechanism. *Journal of Photochemistry and Photobiology A: Chemistry* **152**, 267–273.

Wu, H., Fan, J., Liu, E., Hu, X., Ma, Y., Fan, X., Li, Y. & Tang, C. 2015 Facile hydrothermal synthesis of TiO_2 nanospindles-reduced graphene oxide composite with a enhanced photocatalytic activity. *Journal of Alloys and Compounds* **623**, 298–303.

Xu, Q., Feng, J., Li, L., Xiao, Q. & Wang, J. 2015 Hollow $ZnFe_2O_4/TiO_2$ composites: high-performance and recyclable visible-light photocatalyst. *Journal of Alloys and Compounds* **641**, 110–118.

Zhang, Z., Wan, M. & Mao, Y. 2012 Enhanced photovoltaic effect of TiO_2-based composite $ZnFe_2O_4/TiO_2$. *Journal of Photochemistry and Photobiology A: Chemistry* **233**, 15–19.

Zhang, X., Zhu, Y., Yang, X., Zhou, Y., Yao, Y. & Li, C. 2014 Multifunctional $Fe3O_4$@TiO_2@Au magnetic microspheres as recyclable substrates for surface-enhanced Raman scattering. *Nanoscale* **6**, 5971–5979.

Zhang, J., Liu, P., Lu, Z., Xu, G., Wang, X., Qian, L., Wang, H., Zhang, E., Xi, J. & Ji, Z. 2015 One-step synthesis of rutile nano-TiO_2 with exposed {1 1 1} facets for high photocatalytic activity. *Journal of Alloys and Compounds* **632**, 133–139.

Zhou, W., Liu, H., Wang, J., Liu, D., Du, G. & Cui, J. 2010 Ag_2O/TiO_2 nanobelts heterostructure with enhanced ultraviolet and visible photocatalytic activity. *ACS Applied Materials & Interfaces* **2**, 2385–2392.

Zhu, X., Zhang, F., Wang, M., Ding, J., Sun, S., Bao, J. & Gao, C. 2014 Facile synthesis, structure and visible light photocatalytic activity of recyclable $ZnFe_2O_4/TiO_2$. *Applied Surface Science* **319**, 83–89.

First received 19 May 2023; accepted in revised form 30 June 2023. Available online 29 July 2023